Hindawi Publishing Corporation
Journal of Nanomaterials
Volume 2012, Article ID 628592, 6 pages
doi:10.1155/2012/628592

Research Article

Mineral Phase and Physical Properties of Red Mud Calcined at Different Temperatures

Chuan-sheng Wu[1,2,3] and Dong-yan Liu[1,3]

[1] *College of Civil Engineering, Chongqing University, Chongqing 400044, China*
[2] *College of Civil Engineering, Chongqing Vocational Institute of Engineering, Chongqing 400037, China*
[3] *Laboratory of New Technology for Construction of Cities in Mountain Area, Chongqing University and Ministry of Education, Chongqing 400045, China*

Correspondence should be addressed to Dong-yan Liu, cqudyliu@yahoo.com.cn

Received 9 August 2012; Revised 20 September 2012; Accepted 24 September 2012

Academic Editor: Ming-Guo Ma

Different characterizations were carried out on red mud uncalcined and samples calcined in the range of 100°C–1400°C. In the present paper, the phase composition and structural transition of red mud heated from room temperature are indicated by XRD, TG-DTA, and SEM techniques. The mean particle diameter, density, and bond strength of these samples also have been investigated. The results indicate the decomposition of gibbsite into Al_2O_3 and H_2O between 300°C and 550°C and calcite into CaO and CO_2 in the interval of 600–800°C. Tricalcium aluminate and gehlenite are formed in the range of 800–900°C. Combined with the SEM images, the results of physical property testing show that the particle size and the strength each has a continuous rise during the heat treatment from 150°C to 1350°C. But the value of density will undergo a little drop before 450°C and then increases to a higher value at the temperature of 1200°C. These obtained results provide an important base for the further studies of comprehensive utilization of red mud.

1. Introduction

Red mud is a reddish brown coloured solid waste produced during the physical and chemical processing of bauxite. Bauxite is composed of aluminum hydroxide minerals, including primarily gibbsite ($Al(OH)_3$), boehmite (γ-AlO(OH)), diaspore (α-AlO(OH)), hematite (Fe_2O_3) and goethite (FeO(OH)) [1]. The red mud, according to the production process of the aluminum, can be divided into Bayer process red mud, sintering progress red mud, and combined process red mud. It was reported that there is 0.8~1.5 t of red mud produced by each 1 t alumina produced. Globally, the total amount of red mud produced every year is between 60 and 120 million tons, [2] about 30 million tons of which is produced in China, and the accumulated quantity can reach to 200 million tons in China.

As to the treatment of red mud, stockpiling it in the open yard may lead to serious pollution of the surrounding soil, air, and groundwater. The dike breach at the Ajkai Timfoldgyar Zrt alumina plant in Hungary [3] is warning us to pay enough attention to the comprehensive treatment of the red mud. The comprehensive utilization of red mud can be divided into the following aspects. First, recovery of Fe, Al, Na [4–6], and rare earth elements like Sc, Y, La, Ti, V [6–10] in red mud. Second, reuse of red mud as cement production [11–14] and other construction materials like brick [15, 16], glass [17, 18], and aerated concrete block [19]. Third, utilization of red mud as road base material and filling material in mining [20, 21] and plastic [22]. Forth, application of red mud to absorb heavy metal ions like Cu^{2+}, Zn^{2+}, Ni^{2+}, Cd^{2+} [23–25], and nonmetallic ions and molecules like NO_3^- [26–28] in the wastewater. Fifth, application of red mud can absorb heavy metal ions in the soil [29, 30] and SO_2 in the wastegas [31, 32].

For the purpose of better comprehension utilization of red mud, several studies [33–38] have been carried out on

the physical and chemical properties of red mud under heat treatment. However, most of the above reports on the characterization of red mud have not detailedly research the physical properties from room temperature to an extreme high temperature. The research of SEM diagrams of red mud calcined at different temperature also has not been reported before. In the present paper, the mean particle diameter, density, and bond strength of red mud calcined within the interval 150–1350°C have been investigated. These tests were aimed to correlate phase composition and structural transition of red mud heated from room temperature, which are indicated by XRD, TG-DTA, and SEM techniques. This research is part of a long-term project on the exploitation of the comprehensive utilization of red mud and provides an important base for the further studies of comprehensive utilization of red mud.

2. Materials and Experimental Procedure

2.1. Materials. Red mud samples were collected from an alumina refining plant, in Guizhou, China, the process of which is bauxite-calcination method. Approximately 3–5 kg of red mud samples were collected from six different sites which have been stocked for 3 years. Samples were dried to constant weight at a temperature of 105 ± 5°C for 24 h. Powder batches of about 500 g were calcined for 6 h in at 150, 300, 450, 600, 900, 1050, 1200, 1350°C. Then the samples were removed from the furnace and cooled to room temperature in air. A powder batch of about 500 g was prepared without heat treatment for the use in comparison experiment and TG-DT analysis.

The chemical composition of the uncalcined red mud determined by X-ray fluorescence (XRF-1800X) analyzer is given in Table 1.

2.2. Experimental Methods. X-ray diffraction (XRD) analysis was carried out on a Rigaku (Japan) D/MAX 2500C diffractometer using CuKα radiation, voltage 40 kV, current 200 mA, equipped with a graphite monochromator in the diffracted beam. Crystalline phases were identified using the database of the International Center for Diffraction Data-JCPDS for inorganic substances. (JCPDS, International Centre for Diffraction Data, 1601 Park Line, Swarthmore, PA, 1987).

Thermal analysis was performed on a Netzsch (Germany) STA 449 simultaneous analyzer. Thermogravimetric (TG) and differential thermal (DT) analysis were performed in the range of 50–1450°C (stripping gas: dry N_2, helium flow = 100 mL/min, heating rate: 10°C/min). Measurement were carried out in 0.3 cm^3 volume alumina crucibles using α-alumina as reference, analyzing ≈100 mg of dry sample.

The volume frequency of particle diameter is characterized by a Winner2008A (Chinese) laser particle size analyzer, whose measuring range is 0.05–2000 μm. The density measurements were performed with a helium pycnometer (Micromeritics, Model 1305, USA). And the strength

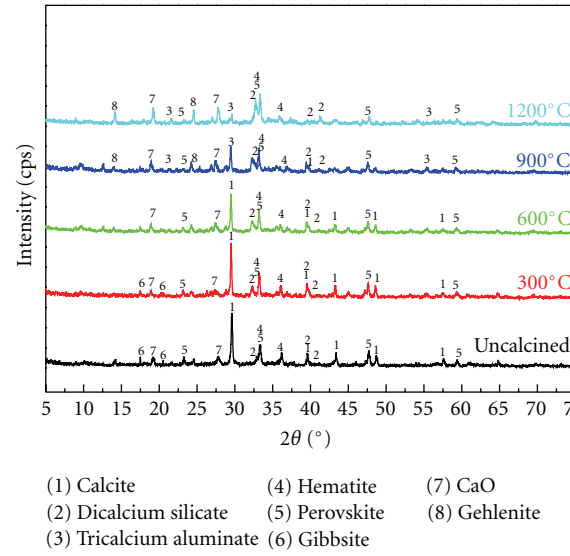

Figure 1: XRD patterns of uncalcined red mud and samples heated at 300°C, 600°C, 900°C, and 1200°C.

performance of red mud calcined at different temperature is tested on a Trautwein DigiShearTM (Chinese) multifunctional direct shear test systems with the following testing condition: the shear rate is 0.03 mm/minute, the maximum shear displacement is 6.5 mm.

SEM observation was performed on TESCAN VEGA II scanning electron microscope for the characterization of the micromorphology of red mud calcined at different temperatures.

3. Results and Discussions

3.1. XRD Analysis. The element analysis and phase characterization of red mud have been reported several times [33, 34, 37, 38]. However, the analysis data of the composition of red mud is not uniform. The XRD patterns of the red mud uncalcined and calcined at the temperatures of 300°C, 600°C, 900°C, 1200°C are shown in Figure 1.

From Figure 1, it can be seen that the main phases in the uncalcined red mud are calcite ($CaCO_3$), dicalcium silicate (Ca_2SiO_4), hematite (Fe_2O_3), perovskite ($CaTiO_3$), gibbsite ($Al(OH)_3$), and CaO. Among these mineral phases, gibbsite cannot be detected in the sample treated over 600°C for the reason of pyrolysis. Calcite is the fundamental phase up to 900°C. Above this temperature, calcite ($CaCO_3$) decrease parallels the increase of CaO and the occurrence of minor components, such as tricalcium aluminate ($Ca_3Al_2O_6$) and gehlenite ($Ca_2Al_2SiO_7$). This indicated the transform of calcite to tricalcium aluminate and Gehlenite and the decomposition of Calcite to CaO in the interval of 600–900°C. Dicalcium silicate (Ca_2SiO_4), hematite (Fe_2O_3), perovskite ($CaTiO_3$), and CaO are not affected by temperature through the process of heating.

Table 1: The main chemical constituents of red mud (%) [38].

Chemical constituent	Fe_2O_3	Al_2O_3	SiO_2	CaO	Na_2O	TiO_2	Sc_2O_3	Nb_2O_5	TREO	Loss
Sintering process	6.66	9.18	18.1	38.09	4	6.72	0.02	0.02	0.25	16.96

3.2. TG-DT Analysis. The TG-DTA diagram (Figure 2) shows a continuous weight loss distributed in the range of 50–1450°C. The figure shows two main portions of mass loss as the rise of temperature. The first one is during the heating temperature interval of 50–550°C when the physically absorbed water and chemically bound water is off. Before the firing temperature is up to 550°C, the sample loses 8.26% total of its weight. The proportion of physically absorbed water is small. Combined with the results of XRD analysis, it can be known that the lost chemically bound water is mainly from the decomposition of gibbsite ($Al(OH)_3$), which is shown as following equation: $Al(OH)_3 \rightarrow Al_2O_3 + H_2O$. But if there are no Al_2O_3 phases detected along with the decrease of $Al(OH)_3$, then Al_2O_3 is believed to have been combined with the CaO (discussed as following) to form tricalcium aluminate or Gehlenite.

Then the mass of the sample undertakes a more rapid decline in the range of 550–900°C with a mass change of 21.81%. As the report [38] says, the main reason is the release of CO_2, which can also be indicated by the XRD pattern in Figure 1. The decrease of Calcite ($CaCO_3$) and the increase of CaO around the temperature of 900°C can prove that the decomposition of $CaCO_3$ is the main source of released CO_2. The chemical equations during this progress are as following: $CaCO_3 \rightarrow CaO + CO_2$, $3CaO + Al_2O_3 \rightarrow Ca_3Al_2O_6$, $2CaO + 2Al_2O_3 + SiO_2 \rightarrow 2Ca_2Al_2SiO_7$. Besides, when the sample is heated at the temperature over 900°C, there is not an obvious mass change.

There are three main endothermic peaks in the DT diagram of red mud. It can be known that the decomposition temperatures of gibbsite to Al_2O_3 and calcite are separately 300–550°C and 600–800°C. And the main reaction temperature of CaO and Al_2O_3 to prepared ricalcium aluminate ($Ca_3Al_2O_6$) is 850–900°C.

Combined the results of XRD analysis and the TG-DT analysis, the phase transition during the heat treatment can be indicated as the following: (1) the main mineral phases of dried red mud at room temperature are calcite ($CaCO_3$), dicalcium Silicate (Ca_2SiO_4), hematite (Fe_2O_3), perovskite ($CaTiO_3$), gibbsite ($Al(OH)_3$), and CaO; (2) in the range of 300–550°C, the gibbsite decomposes into Al_2O_3 and H_2O; (3) at the temperature of 600–800°C, the calcite decomposes into CaO and CO_2; (4) the phases of tricalcium aluminate ($Ca_3Al_2O_6$) and gehlenite ($Ca_2Al_2SiO_7$) start to emerge in the 800–900°C interval; (5) there is no obvious mass change or phase change above 900°C.

3.3. Physical Properties Testing. The physical properties such as particle size, density and strength change as the increase of the calcined temperature of red mud.The particles size

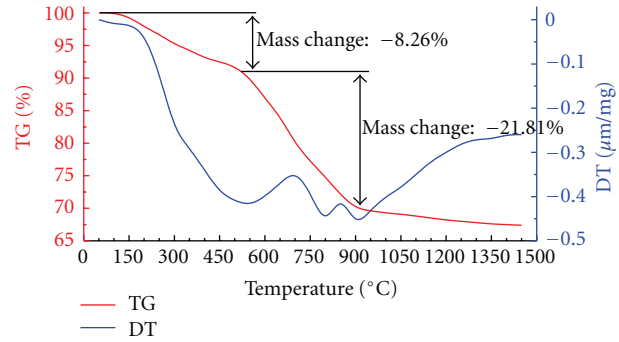

Figure 2: Thermogravimetric (TG) and differential thermal (DT) analysis diagram of dried red mud.

distribution of the uncalcined red mud is shown in Figure 3(a). It can be seen that the ground red mud particles are mostly in the range of 1–80 μm with a mean value of 26.7 μm. But it will be different as the change of calcined temperature, which can be indicated from the Figure 2(b). With the firing temperature from 150°C to 1350°C, the average particle diameter of red mud rises from 26.7 μm to 38.2 μm. The increase of the particle size may influenced the improvement of crystallization. From the XRD pattern (Figure 1), it can be known that, except the vanishing phases like calcite and gibbsite, the crystallinities of the majority of phases of red mud are improved by heat treatment. This will promote the rising of the mean particle diameter value.

The density of red mud at room temperature is 3.26 g/cm^3, which will change as the red mud is under heat treatment. The bond strength of uncalcined red mud tested by the direct shear test systems is 322 kPa. The values of density and bond strength change as the functions of temperature are shown in Figure 4. From the diagram we can know the following aspects. The value of density decrease until the temperature is 450°C, which is in contrast to the change of bond strength. Then they both increase obviously from 450°C to 1200°C and decline a little when the temperature is higher than 1200°C. The maximum values of density and bond strength are 3.41 cm^3 and 452 kPa at 1200°C.

These phenomenons can also be explained by the XRD analysis result like the change of mean particle diameter value. The enhancement of strength properties may result from the improvement of crystallinities of major phases and the appearance of high strength phases like tricalcium aluminate and gehlenite. While as to the change of density, the decline before 450°C is determined by the emission of water and the decomposition of gibbsite ($Al(OH)_3$,

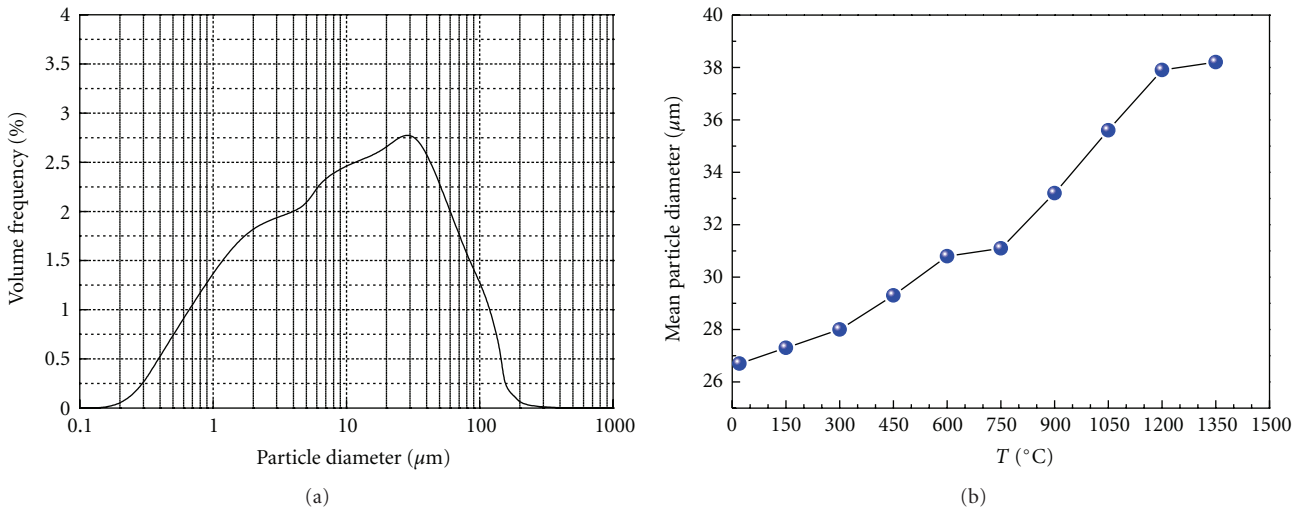

Figure 3: (a) Particle size distribution of red mud at room temperature; (b) mean particle size at different calcined temperatures.

2.42 g/cm^3) to Al_2O_3 (3.97 g/cm^3) and calcite ($CaCO_3$, 2.60~2.80 g/cm^3) to CaO (3.25~3.38 g/cm^3).

3.4. SEM Analysis. For the purpose of further comprehension the phase change progress of red mud during heat treatment, red mud uncalcined, and samples calcined at 150°C, 450°C, 600°C, 900°C, and 1200°C are dispersed in anhydrous alcohol and grinded by ultrasonic vibration for the same time (24 h). Then the samples were observed by scanning electron microscope to obtain the micromorphology maps of these samples. The SEM images of red mud uncalcined and calcined are showed in Figure 5.

From Figure 5(a) it can be known that the microscopic structure of uncalcined red mud is relatively loose, with high porosity and small particle size. On the contrary, the diagrams of red mud calcined at a serious of temperatures (Figures 5(b)–5(e)) indicate that the heat treatment can improve the value of particle diameter and make the particles easy to gather with each other. The increasing tendency of particle size is consistent to the values measured by laser particle size analyzer as shown in Figure 3(b).

Different microstructures result from different physical and chemical progresses. With the influence of heating at 150°C, red mud loses the majority of its physically absorbed water and part of chemically bound water. So Figure 5(b) presents large particles and a high porosity, corresponding to a low density as shown in Figure 4. When calcined at 450°C, with the decomposition of phases like gibbsite, red mud has lost almost all the chemically bound water. So it can have larger particle and higher porosity (also lower density) than calcined at 150°C (Figure 5(c)). Density of red mud is determined by two main different factors: porosity and particle size. When firing at 600°C, 900°C, and 1200°C, there is no water emission that leads to the variation of porosity. But the phase transition and improvement of crystalline degree can make the increase of particle diagram significant (Figures 5(e)–5(f)). Therefore red mud can have a gradually increasing value of density.

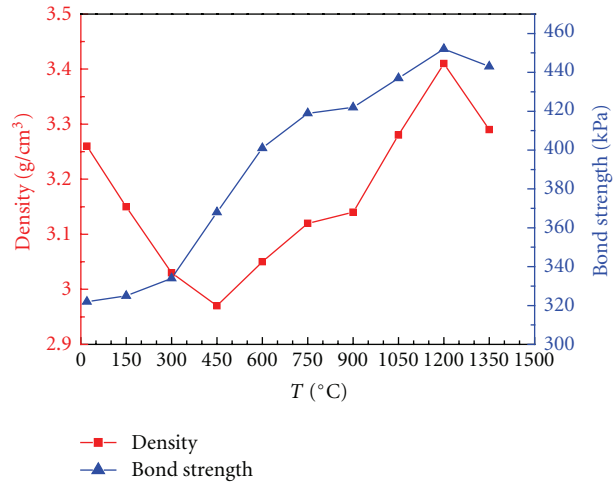

Figure 4: Changes of density and bond strength as the functions of calcined temperature.

4. Conclusion

In this paper, through the XRD and TG-DT analysis, the phase transition during the heat treatment contained the following several progresses: (1) gibbsite decomposes into Al_2O_3 and H_2O (300–550°C); (2) calcite decomposes into CaO and CO_2 (600–800°C); (3) the emergence of Tricalcium aluminate ($Ca_3Al_2O_6$) and gehlenite ($Ca_2Al_2SiO_7$) (800–900°C). From the results of physical property testing and SEM analysis, it can be indicated that the physical properties of red mud have the obvious variations during the progress of firing of red mud. The particle size and the strength each has a continuous rise during the heat treatment from 150°C

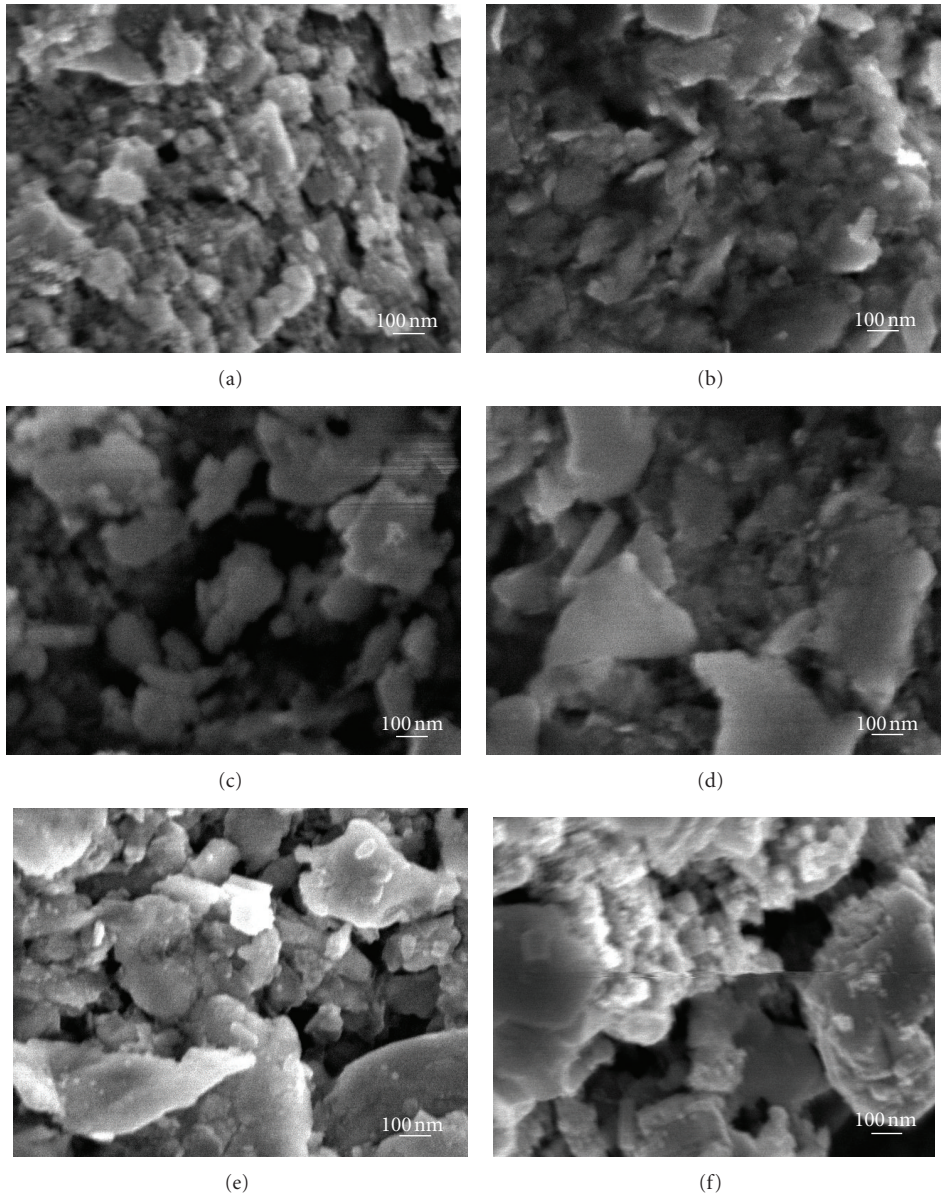

Figure 5: The SEM images of red mud (a) uncalcined and calcined at (b) 150°C, (c) 450°C, (d) 600°C, (e) 900°C, and (f) 1200°C.

to 1350°C, because of the improvement of crystallinities of major phases and the appearance of high strength phases like tricalcium aluminate and gehlenite. But as to the value of density, it will undergo a little drop before 450°C as an effect of the increase of porosity, and then increases to a new high value at the temperature of 1200°C. All the obtained results will provide an important base for the further studies of comprehensive utilization of red mud.

References

[1] Mineral Photos—Aluminum &Bauxite Homepage, 2012, http://www.mii.org/Minerals/photoal.html.

[2] P. Renfortha, W. M. Mayesb, A. P. Jarvisc, I. T. Burked, D. C. Manningc, and K. GruizeScience, "Contaminant mobility and carbon sequestration downstream of the Ajka (Hungary) red mud spill: the effects of gypsum dosing," *Science of the Total Environment*, vol. 421-422, pp. 253–259, 2012.

[3] H. J. Reeves, G. Wealthall, and P. L. Younger, "Advisory Visit to the Bauxite Processing Tailings Dam near Ajka, Vesprem County, Western Hungary," Open Report OR/11/006, British Geological Survey, Keyworth, UK, 2011.

[4] Y. F. Sun, F.Z. Dong, and J.T. Liu, "Technology for recovering iron from red mud by Bayer process," *Metal Mine*, vol. 9, pp. 176–178, 2009 (Chinese).

[5] L. Zhong and Y. F. Zhang, "Sub molten salt method recycling red mud," *The Chinese Journal of Nonferrous Metals*, vol. 18, pp. 70–73, 2008.

[6] X. F. Zheng, "Recycling technology of aluminum and sodium from low temperature bayer progress red mud," *Shandong Metallurgy*, vol. 32, pp. 16–17, 2010.

[7] P. M. Orhsenkiihnn, T. Lybempudu, and K. M. Ochsenkiihn, "ReCovery of lmththanides and yttrium from red mud by selective leaching," *Analytica Chimica Acta*, vol. 319, pp. 249–254, 1996.

[8] M. Ochsenkühn-Petropulu, T. Lyberopulu, and G. Parissakis, "Selective separation and determination of scandium from yttrium and lanthanides in red mud by a combined ion exchange/solvent extraction method," *Analytica Chimica Acta*, vol. 315, no. 1-2, pp. 231–237, 1995.

[9] D. I. Smirnov and T. V. Molchanova, "The investigation of sulphuric acid sorption recovery of scandium and uranium from the red mud of alumina production," *Hydrometallurgy*, vol. 45, no. 3, pp. 249–259, 1997.

[10] X. H. Chen, Y. Chen, M. Gan, and K. X. Xu, "Precipitation and separation of vanadium from bayer process sodium aluminate solution," *The Chinese Journal of Process Engineering*, vol. 10, pp. 24–38, 2010.

[11] X. R. Qiu and Y. Y. Qi, "The reasonable utilization of red mud in cement production," *Cement Technology*, vol. 6, pp. 103–105, 2011.

[12] E. Kalkan, "Utilization of red mud as a stabilization material for the preparation of clay liners," *Engineering Geology*, vol. 87, no. 3-4, pp. 220–229, 2006.

[13] A. A. Barsherike, *New Cement*, Edited by Y. Y. Qian, China Building Industry Press, Beijing, China, 1983.

[14] I. Vangelatos, G. N. Angelopoulos, and D. Boufounos, "Utilization of ferroalumina as raw material in the production of Ordinary Portland Cement," *Journal of Hazardous Materials*, vol. 168, no. 1, pp. 473–478, 2009.

[15] A. P. Yang, "The development of brick made of red mud and fly ash," *Light Metals*, vol. 12, pp. 17–18, 1996.

[16] N. Yalçin and V. Sevinç, "Utilization of bauxite waste in ceramic glazes," *Ceramics International*, vol. 26, no. 5, pp. 485–493, 2000.

[17] J. K. Yang, D. D. Zhang, and B. Xiao, "Study on glass-ceramics mostly made from red mud and fly ash," *Glass & Enamel*, vol. 32, pp. 9–11, 2004 (Chinese).

[18] Z. Y. Liang, "The research on black glass decorative materials made from red mud," *Environmental Protection of Chemical Industry*, vol. 18, pp. 50–51, 1998.

[19] B. Wu, D. C. Zhang, and Z. Z. Zhang, "The study of producing aerated-concrete blocks from red-mud," *China Resources Comprehensive Utilization*, vol. 6, pp. 29–31, 2005.

[20] L. G. Yang, Z. L. Yao, and D. S. Bao, "Pumped and cemented red mud slurry filling mining method," *Mining Research and Development*, vol. 16, pp. 18–22, 1996.

[21] H. M. Wang, "The comprehensive utilization of red mud," *Shanxi Energy and Conservation*, vol. 11, pp. 58–61, 2011.

[22] X. L. Nan, T. A. Zhang, Y. Liu, and Z. H. Dou, "Analysis of comprehensive utilization of red mud in China," *The Chinese Journal of Process Engineering*, vol. 10, no. 1, pp. 264–270, 2010.

[23] M. Vaclavikova, P. Misaelides, G. Gallios, S. Jakabsky, and S. Hredzak, "Removal of cadmium, zinc, copper and lead by red mud, an iron oxides containing hydrometallurgical waste," *Studies in Surface Science and Catalysis*, vol. 155, pp. 517–525, 2005.

[24] M. Erdem, H. S. Altundoğan, and F. Tümen, "Removal of hexavalent chromium by using heat-activated bauxite," *Minerals Engineering*, vol. 17, no. 9-10, pp. 1045–1052, 2004.

[25] L. Santona, P. Castaldi, and P. Melis, "Evaluation of the interaction mechanisms between red muds and heavy metals," *Journal of Hazardous Materials*, vol. 136, no. 2, pp. 324–329, 2006.

[26] Y. Çengeloğlu, E. Kir, and M. Ersöz, "Removal of fluoride from aqueous solution by using red mud," *Separation and Purification Technology*, vol. 28, no. 1, pp. 81–86, 2002.

[27] G. Akay, B. Keskinler, A. Çakici, and U. Danis, "Phosphate removal from water by red mud using crossflow microfiltration," *Water Research*, vol. 32, no. 3, pp. 717–726, 1998.

[28] H. S. Altundoan, S. Altundoan, F. Tümen, and M. Bildik, "Arsenic adsorption from aqueous solutions by activated red mud," *Waste Management*, vol. 22, no. 3, pp. 357–363, 2002.

[29] R. Ciccu, M. Ghiani, A. Serci, S. Fadda, R. Peretti, and A. Zucca, "Heavy metal immobilization in the mining-contaminated soils using various industrial wastes," *Minerals Engineering*, vol. 16, no. 3, pp. 187–192, 2003.

[30] E. Lombi, F. J. Zhao, G. Wieshammer, G. Zhang, and S. P. McGrath, "*In situ* fixation of metals in soils using bauxite residue: biological effects," *Environmental Pollution*, vol. 118, no. 3, pp. 445–452, 2002.

[31] Z. Bekir, A. Inci, and Y. Hayrettin, "Sorption of SO_2 on metal oxides in a fluidized bed," *Industrial and Engineering Chemistry Research*, vol. 27, no. 3, pp. 434–439, 1988.

[32] G. Z. Lu, T. A. Zhang, L. Bao, Z. H. Dou, and W. G. Zhang, "Roasting pretreatment of high-sulfur bauxite," *The Chinese Journal of Process Engineering*, vol. 8, no. 5, pp. 892–896, 2008.

[33] V. M. Sglavo, R. Campostrini, S. Maurina et al., "Bauxite "red mud" in the ceramic industry—part 1: thermal behaviour," *Journal of the European Ceramic Society*, vol. 20, no. 3, pp. 235–244, 2000.

[34] Y. Zhang and Z. Pan, "Characterization of red mud thermally treated at different temperatures," *Journal of Jinan University for Science and Technology*, vol. 19, pp. 293–297, 2005 (Chinese).

[35] V. Jobbágy, J. Somlai, J. Kovács, G. Szeiler, and T. Kovács, "Dependence of radon emanation of red mud bauxite processing wastes on heat treatment," *Journal of Hazardous Materials*, vol. 172, no. 2-3, pp. 1258–1263, 2009.

[36] S. Srikanth, A. K. Ray, A. Bandopadhyay, B. Ravikumar, and A. Jha, "Phase constitution during Sintering of red mud and red mud-fly ash mixtures," *Journal of the American Ceramic Society*, vol. 88, no. 9, pp. 2396–2401, 2005.

[37] H. Chen, H. Sun, and H. Li, "Effect of heat treatment temperature on cementitious activity of red mud," *Light Metals*, vol. 9, pp. 22–25, 2006 (Chinese).

[38] X. Liu, N. Zhang, H. Sun, J. Zhang, and L. Li, "Structural investigation relating to the cementitious activity of bauxite residue—red mud," *Cement and Concrete Research*, vol. 41, no. 8, pp. 847–853, 2011.